



Enhanced production of phenolics and aromatics from raw bio-oil using HZSM-5 zeolite additives for PtPd/C and NiW/C catalysts



Idoia Hita^{a,*}, Tomás Cordero-Lanzac^a, Francisco J. García-Mateos^b, M. Josune Azkoiti^a, José Rodríguez-Mirasol^b, Tomás Cordero^b, Javier Bilbao^a

^a Department of Chemical Engineering, University of the Basque Country (UPV/EHU), PO Box 644-48080, Bilbao, Spain

^b Universidad de Málaga, Department of Chemical Engineering, Andalucía Tech., Campus de Teatinos s/n, 29010 Málaga, Spain

ARTICLE INFO

Keywords:

Hydrodeoxygenation
Activated carbon catalyst
Zeolite
Aromatics
Phenolics

ABSTRACT

This study delves into the performance of a Pt-Pd and a Ni-W catalyst supported on a phosphorus-containing activated carbon (ACP) in the hydrodeoxygenation (HDO) of raw bio-oil, as well as the enhancement of phenolic and aromatic product yields produced by incorporating physically mixed HZSM-5 zeolites (20 wt%) of different Si/Al ratio (15 and 140 in zeolites Z15 and Z140, respectively) in the catalytic bed. The HDO runs have been conducted in a fixed bed reactor at: 450 °C; 65 bar; space time, 0.15 g_{cat} h g_{bio-oil}⁻¹; 90 ml min⁻¹ H₂; and time on stream up to 6 h. After a fast initial deactivation due to coke deposition the catalysts reached a pseudosteady state at which the carbon product yields are higher than in fresh catalyst conditions. The NiW catalyst provided yields of 42.3 wt% liquid carbon products (in a dry bio-oil basis), yielding 5.3 wt% phenolic and 12.3 wt% aromatic product yields. The NiW + Z140 combination was the most efficient catalyst (with a 47.3 wt% carbon production, including 6.8 wt% phenolics and 15.5 wt% aromatics) as a consequence of this low-acidity zeolite promoting the synergy with the dehydrogenation activity of metallic sites by favoring the acid-catalyzed cracking reactions of the bio-oil oxygenates, while simultaneously limiting gas product and coke formation. Two types of coke were detected, of thermal origin and catalytic coke, with the formation of the latter being dependent on the acidity of the zeolite.

1. Introduction

Biomass-derived feedstock is attracting great research interest due to the foreseeable midterm depletion of fossil resources and increasing strict environmental policies. Specifically, fast pyrolysis of biomass offers promising possibilities given its limited environmental impact, and great potential for the valorization of the resulting products at an industrial refinery scale, particularly the liquid fraction which is known as bio-oil [1,2].

Bio-oil is a highly complex mixture of water (up to 50%, depending on the biomass source [3]) and a wide array of organic oxygenates which originate from the depolymerization of holocellulose (comprising cellulose and hemicellulose) and lignin. A detailed classification of the oxygenates present in bio-oil would distinguish phenols, ketones, acids, esters, aldehydes, alcohols, furans, anhydrous-sugars, nitrogen-containing compounds, and carboxylic acids [4]. Its low stability, high viscosity, corrosiveness and difficulty of storage prevent its wider application as a fuel and, therefore, the necessity to adequate its composition has boosted the research of a number of upgrading routes (i.e.

steam reforming [5,6], catalytic cracking and hydroprocessing [7]). The hydrodeoxygenation (HDO) approach outstands for providing stabilized bio-oil with enhanced fuel applications [8], and high-quality products, as phenolics and aromatics. The main sets of reactions that take place in the HDO of bio-oil are: C–O bond hydrogenolysis, dehydration, decarboxylation, hydrogenation of unsaturated components and C–C bond cleavage [9].

So far, HDO has primarily been explored over conventional sulfided transition metals comprising Ni, Mo, Co, W and/or combinations of these. Nonetheless, the high tendency towards coke formation of these catalysts, as well as the necessity to add an external sulfur source to the reaction media for their activation, direct catalyst preference towards noble metal-based catalysts (i.e. Ru, Rh, Pd, Pt, or bimetallic combinations) which, in addition, provide a higher activity at milder operation conditions [7]. The addition of a second metal can avoid problems with Pd sintering [10]. On the other hand, PtPd catalysts perform stably during hydroprocessing, with a higher hydrogenation activity than the monometallic Pt and Pd counterparts [11].

Given the complexity of unraveling the catalytic conversion of real

* Corresponding author.

E-mail address: idoia.hita@ehu.eus (I. Hita).

bio-oil, model components have been primarily targeted in order to understand the basic HDO processes [12,13]. Auersvald et al. [14] have established the following bio-oil component reactivity order on the HDO of bio-oil over a NiMo catalyst: aldehydes, syringols, guaiacols, benzenediols, esters/lactones, ketones, alcohols, furans, carboxylic acids and mono-hydroxy-benzenes. However, more recently an important number of works dealing with real bio-oil feedstock are providing greater insights into its HDO conversion, aiming for transportation fuels and chemicals [7,15,16]. Studies on a wide range of catalyst supports have shown the crucial role of their physico-chemical features (namely porosity and acidity) in HDO reactions, particularly on the conversion of bulkier and highly refractory components. Among the supports, works on SiO_2 [17], $\text{SiO}_2\text{-Al}_2\text{O}_3$ [18], TiO_2 [19], ZrO_2 [10], zeolites [20] and carbon [16,21,22] are the most reported.

Carbonaceous materials are one of the most studied alternatives as catalyst support due to their low cost and sustainable origin [23]. In fact, commercial C-supported noble metal catalysts are widely extended for HDO reactions [24,25]. However, different configurations of activated carbons (ACs) have been reported to enhance the catalytic performance as a consequence of the best metal dispersion in a well-developed amorphous structure [26]. The functionalization of carbon surface can also provide the catalyst with an acidic function that contributes into the advance of the HDO mechanism. In a previous work, the stability of a P-functionalized AC (ACP)-based bifunctional PtPd catalyst was demonstrated by Cordero-Lanzac et al. [9] on the hydrodeoxygenation of raw bio-oil. After the fast initial deactivation, the presence of hydrothermally resistant acidic sites yielded high selectivity to aromatics, and also allowed for maintaining a pseudosteady state of the catalyst [9,23].

In an analogue way to ACs, zeolite/zeolitic materials offer ample possibilities for being tailored and adapted to the requirements of bio-derived feedstock upgrading [27], and have been explored as interesting catalysts in the catalytic pyrolysis of biomass for maximizing the production of high-quality bio-oils [28]. Valle et al. [29] and Shakya et al. [30] demonstrated the capability of a Ni/HZSM-5 catalyst for selectively producing aromatic components in the cracking/deoxygenation of bio-oil into hydrocarbons. The HZSM-5 zeolite presents a high hydrothermal stability, and the limiting size of the MFI structure channels ($5.1 \times 5.5 \text{ \AA}$) selectively favors the production of phenolics and one-ring aromatics from biomass [31]. Moreover, its straight and zigzagged channels without cages allow the diffusion of the aromatic compounds towards the reaction medium, delaying the formation of catalytic coke from bio-oil [32].

Motivated by all the previous, the aim of this study is to explore the performance of a NiW and a PtPd catalyst supported on an ACP on the hydrodeoxygenation of a raw bio-oil and also the effect of the addition of a physically mixed HZSM-5 zeolite in the catalyst bed on the liquid product composition. Specifically, the enhancement of phenolic and aromatic component yields is pursued, given their crucial role in future biorefineries [33]. The production capacity of these chemicals has been compared for the different catalysts once the pseudosteady state was reached. Lastly, the used catalysts have been characterized by temperature-programmed oxidation (TPO), X-ray photoelectron spectroscopy (XPS), N_2 adsorption-desorption and CO_2 adsorption. These analyses provided insights into the nature and content of coke, its location in the porous structure and the effect of its deposition in the catalyst properties.

2. Experimental

2.1. Catalyst preparation

Two bifunctional catalysts were prepared, supported on a phosphorus-containing activated carbon (ACP), and with Pt-Pd or Ni-W combinations as metallic functions. The selection of the Pt-Pd catalyst is justified by its good performance in a previous work [9] and the Ni-W

originally proposed in this work as a lower-cost alternative, given the good performance of NiW catalysts in hydroprocessing reactions [34,35]. The ACP supports were obtained from the chemical activation of olive stone [36]. In the first place, olive stones were impregnated with H_3PO_4 (85 wt%, 3 g of H_3PO_4 per g of precursor) and then activated under a N_2 atmosphere ($150 \text{ cm}^3 \text{ min}^{-1}$) in a tubular furnace at 500°C for 2 h increasing temperature at a $10^\circ\text{C min}^{-1}$ rate. The obtained activated carbon was subsequently cooled in the tubular furnace, washed with distilled water at 60°C (until no phosphate was detected in the eluent), and finally dried in a vacuum drier at 100°C for 12 h. The ACP was then sieved to a particle size of $100\text{--}300 \mu\text{m}$. Pt (1 wt%) and Pd (0.5 wt%) were incorporated simultaneously through incipient wetting of an aqueous solution of Pt(II) acetylacetone and PdCl_2 slightly acidified with HCl. On the other hand, the same methodology was used for incorporating Ni (5 wt%) and W (2 wt%) using an aqueous solution of $\text{Ni}(\text{NO}_3)_2 \cdot 6\text{H}_2\text{O}$ and $(\text{NH}_4)_6\text{W}_7\text{O}_{24} \cdot 6\text{H}_2\text{O}$. The impregnated supports were heat-treated in a tubular furnace under a N_2 flow ($150 \text{ cm}^3 \text{ min}^{-1}$) at 400°C for 4 h. Each fresh catalyst was designated based on the bimetallic function deposited on the ACP support: PtPd and NiW.

Commercial HZSM-5 zeolites with Si/Al ratio of 15 and 140 (provided by Zeolyst in their ammonium form) were pretreated at 100°C during 6 h and then calcined in a muffle oven at 575°C for 2 h. Subsequently, zeolites were tableted and sieved to a particle size of $300\text{--}500 \mu\text{m}$. The zeolites were designated on the basis of their Si/Al ratio (15 and 140), as Z15 and Z140, respectively.

2.2. Catalyst characterization

The porous structure of the fresh and used ACP-based catalysts and the zeolites were analyzed by means of N_2 adsorption-desorption at -196°C and CO_2 adsorption at 0°C in a Micromeritics ASAP 2020 equipment. Prior to the analysis, samples were degassed for 8 h at 50°C in vacuum conditions in order to avoid the extraction of some deactivating species from within the used catalyst pores under vacuum. From the obtained isotherms, the specific surface area (S_{BET}) was computed using the BET equation, while the micropore volume (V_{micr}) and the external surface area (S_{ext}) were calculated using the t -method. The mesopore volume (V_{mes}) was computed by the difference between the total pore volume and the V_{micr} . The BJH method was applied for estimating the average pore size (d_{pore}). On the other hand, the narrow micropore surface area (S_{DR}) was computed from the CO_2 adsorption isotherm using the Dubinin-Radushkevich equation.

Acidic properties of the ACP supports and zeolites were measured by temperature-programmed desorption (TPD) of *tert*-butylamine (tBA) at 500°C with a heating rate of 5°C min^{-1} , after a previous adsorption at 100°C , in a Setaram DSC thermogravimetric calorimeter unit coupled online with a Balzers Quadstar 422 mass spectrometer. Samples were previously stripped under a He atmosphere at 550°C . The recorded mass during the TPD was the one associated with butene ($m/z = 56$), thus estimating the acidity of these sites capable of cracking hydrocarbon molecules.

Transmission electron microscopy (TEM) analyses were carried out in a Philips CM200 microscope provided with a supertwin lens to study the morphology of the catalyst. The metal particle size was calculated by counting particles in five different micrographs for each catalyst.

X-ray photoelectron spectroscopy (XPS) was used for studying the chemical surface composition and elemental identity of the catalysts in a 5700C model Physical Electronics apparatus with $\text{MgK}\alpha$ radiation (1253.6 eV). The C1s peak was located at 284.5 eV [37] and it was used as reference to locate the other peaks. Fitting of XPS peaks was done by least squares using Gaussian-Lorentzian peak shapes.

The total amount of each metal in the fresh catalysts was measured by inductively coupled plasma high resolution mass spectrometry (ICP-MSHR). Samples (ca. 100 mg) were dispersed into a $\text{HNO}_3\text{/H}_2\text{O}_2\text{/HF}/\text{H}_3\text{BO}_3$ solution with a volume ratio of 6/2/1/5, respectively. The

digestion of the mixture was carried out in a microwave furnace at 40 bar and 240 °C. Finally, an Element XR (Thermo Fisher) apparatus was used to measure the metal contents.

The deposited coke content in the used catalysts was measured by means of combining thermogravimetric techniques with a temperature-programmed oxidation (TG-TPO) in a TA Instruments TGA Q5000 IR apparatus. The measurements were performed at least three times for assuring their reproducibility. The relative amounts of the different coke types were calculated from a Lorentzian deconvolution of the DTG-TPO profiles using a MATLAB® routine.

2.3. Bio-oil

The raw bio-oil was obtained from the fast pyrolysis of black poplar sawdust at 450–550 °C in a pilot plant provided with a conical spouted bed reactor (CSBR) with a capacity of 25 kg h⁻¹ [38]. Its elemental composition (CHN) was determined through elemental analysis in a Leco TruSpec CHN Macro provided with an additional TruSpec S module, and the oxygen content was determined by difference. The water content was measured by Karl-Fischer titration in a Metrohm830 KF Titrino plus apparatus. The chemical composition of the bio-oil was analyzed by means of GC-MS in a Shimadzu GC-MS QP2010 unit provided with a BPX5 column (length, 50 m; internal diameter, 0.22 mm). The elemental and chemical compositions of the raw black poplar bio-oil used in this work have already been detailed in a previous work [9]. A predominance of oxygenated components was observed, particularly acetic acid (23.5 wt%), levoglucosan (24.0 wt%) and phenolic components (13.0 wt%) which comprise alkylphenolic and alkylmethoxyphenolic components, known to be highly unstable and reactive towards repolymerizing and further evolving into coke [23].

2.4. Hydroprocessing unit, product analysis and reaction parameters

The raw bio-oil hydroprocessing runs were carried out in a down-flow fixed bed reactor schematized in detail elsewhere [39], and operating in a trickle bed regime under the following conditions: 450 °C; 65 bar; space time, 0.15 g_{cat} h g_{bio-oil}⁻¹; 90 ml min⁻¹ H₂; and time on stream, 0–6 h. The catalyst, diluted in SiC, was loaded in the reactor as described by Van Herk et al. [40] in order to avoid heat losses and gas bypassing. Mixtures of ACP-based catalysts (80 wt%) and HZSM-5 zeolites (20 wt%) were also tested at the same conditions (the space time was referred to the total catalyst amount). Prior to the reaction, the catalysts were reduced at 400 °C for 4 h under a continuous gas flow mix of 30 ml min⁻¹ H₂ and 50 ml min⁻¹ N₂. After exiting the reactor, the reaction products were sent to a gas/liquid separator from where they were collected and weighed every hour for mass balance calculation purposes, while gases were collected and analyzed in a Varian 490 microGC, provided with 4 channels: (i) a molecular sieve to separate the permanent gases H₂, O₂, N₂, methane and CO; (ii) a Porapak Q to separate CO₂ and water; (iii) a Al₂O₃ to separate C₂–C₅ hydrocarbons; and (iv) a Stabilwax to separate C₆–C₈ hydrocarbons, methanol and BTX aromatics.

After exiting the reactor and prior to sample collection, liquid reaction products (2.1–2.4 ml h⁻¹, depending on the catalytic system) were contained in a Peltier cell where they cool down and volatiles condense. Once liquid products were collected, both the organic and aqueous phases were easily separated by decantation for their individual analysis without assuming significant experimental error. The organic product phase was analyzed through two-dimensional Gas Chromatography (GCxGC) coupled with Mass Spectrometry (MS) in an Agilent 7890A apparatus connected in line with an Agilent 5975C series MS. The GCxGC consists of two columns of different polarities connected through a flow modulator, being the first column a non-polar DB-5MS (length, 30 m; internal diameter, 0.25 mm), while the second one was a polar TRB-50 HT (length, 5 m; internal diameter, 0.25 mm). On the other hand, the aqueous phase was analyzed using the

previously described Shimadzu GC-MS QP2010. Likewise, the water content in the aqueous product phase was determined by Karl-Fischer titration (Metrohm830 KF Titrino plus).

The liquid carbon product (C-prod) and water yields were defined as specified in Eq. (1) on a total bio-oil basis (including water), while the gas + coke yield was calculated by difference.

$$Y_{i,\text{wet basis}} = \frac{F_i}{F_{\text{total bio-oil}}} \cdot 100 \quad (1)$$

where F_i and F_{total bio-oil} are hourly mass flows of the product fractions and the total bio-oil, respectively.

The hydrocarbon products have been grouped in different lumps, as follows: oxygenates (comprising methanol, acetone and acetic acid), alkanes, ketones, phenol, phenolics, 1-ring aromatics (A₁), 2⁺-ring aromatics (A₂₊) and other oxygenates (acids and esters). Their yields on a dry basis are defined by Eq. (2) as:

$$Y_{i,\text{dry basis}} = \frac{F_i}{F_{\text{bio-oil oxygenates}}} \cdot 100 \quad (2)$$

where F_i and F_{bio-oil oxygenates} refer to the hourly mass flows of each hydrocarbon lump and the oxygenates in bio-oil (excluding water), respectively.

3. Results

3.1. Properties of the fresh catalysts

The main physico-chemical properties of the fresh catalysts are summarized in Table 1. The displayed structural parameters are calculated from the N₂ adsorption–desorption isotherms of Fig. S1. The bare ACP support and ACP-based catalysts show type IV isotherms, associated with mesoporous materials. The incorporation of the metallic phase barely affects the porous structure of the ACP support in the case of the PtPd catalyst, which shows the most developed micro- and mesoporous structure with a S_{BET} of 1380 m² g⁻¹ and significant values of V_{micr} and V_{mes} (0.53 and 0.60 cm³ g⁻¹, respectively). On the other hand, the NiW phase impregnation provokes a partial blockage of the ACP pores, thus observing a decrease in the S_{BET}, V_{micr} and V_{mes}. A pronounced drop of the amount of N₂ adsorbed in the micropore range (low relative pressures) and mesopores (lower isotherm slope at higher relative pressures) is observed in Fig. S1 for the NiW catalyst. This is a direct consequence of the higher amount of loaded metal in this catalyst. Both Z140 and Z15 zeolites exhibit similar isotherm shapes, typical of microporous materials. Nevertheless, their porous structures present lower development than that of the ACP support (S_{BET} of 485 and 509 m² g⁻¹, respectively). Thereby, the physical mixture of zeolites

Table 1
Physico-chemical properties of the fresh catalysts.

	PtPd	NiW	Z140	Z15
Textural parameters				
S _{BET} (m ² g _{cat} ⁻¹)	1380	886	485	509
V _{micr} (cm ³ g _{cat} ⁻¹)	0.53	0.28	0.20	0.19
V _{mes} (cm ³ g _{cat} ⁻¹)	0.60	0.33	0.16	0.22
d _{pore} (Å)	58	56	74	81
XPS surface concentration				
O (wt%)	8.3	12.2	nm ^a	nm ^a
P (wt%)	2.4	1.9	–	–
Pt (wt%)	1.2	–	–	–
Pd (wt%)	0.5	–	–	–
Ni (wt%)	–	4.5	–	–
W (wt%)	–	1.7	–	–
Acidic properties				
Total acidity (mmol _I BA g ⁻¹)	0.38 ^b	0.28 ^b	0.41	0.82
Average strength (kJ mol _I BA ⁻¹)	68 ^b	70 ^b	112	150

^a nm: not measured.

^b Corresponding to the ACP support.

with ACP-based catalysts decreases the adsorbed N₂ on the micropores, but being equal on the mesopores.

According to XPS analyses, some O and P functionalities are anchored on the ACP surface after the preparation treatment. Regarding the O/P ratio, most of these functional groups should be phosphate type, as we observed in a previous work [41]. In the case of the NiW catalyst, the increase in this ratio could be due to a higher formation of metal-oxygen surface groups, which presumably evolve towards the metallic state after the reduction pretreatment of the catalyst. XPS analyses also show similar concentrations to the nominal loads on the surface of the ACP-based catalysts (Table 1) for Pt (1 wt%), Pd (0.5 wt %), Ni (5 wt%) and W (2 wt%), which indicates that most of these metal particles are well-dispersed on the surface of the support. ICP-MSHR analyses were carried out in order to corroborate the total amount of metals incorporated in each catalyst. Results reveal contents of Pt and Pd of 0.8 and 0.4 wt% in the PtPd catalyst and contents of Ni and W of 3.8 and 1.5 wt% in the NiW catalyst, respectively. XPS analyses allow for analyzing the surface concentration (ca. 20 Å deep into the catalyst particle surface), providing metal concentration values higher in all cases than those obtained by means of ICP-MSHIR. This highlights that the metal particles are mainly located in the accessible surface of the catalyst, where they are more likely to be exposed to reactants.

TEM images of the fresh PtPd and NiW catalysts are displayed in Fig. 1a and b, respectively. Well-dispersed nanoparticles are observed in both cases, with a lower density of metal in the case of PtPd catalyst. This was expected regarding the much lower metal loading in this catalyst. From different TEM images of each catalyst, their particle size distributions were estimated (Fig. 1c and d, for PtPd and NiW catalysts,

respectively). A peak maximum is observed in the particle size distribution of PtPd, with an average particle size of 11.8 ± 0.3 nm according to the frequency of each contribution. On the contrary, a broader distribution is shown by the NiW catalyst even though the maximum is clearly shifted towards lower values (7.5 nm). The higher contribution of particles bigger than 12 nm in this catalyst could explain the previously discussed higher blockage of the support pores (see Table 1). Nevertheless, its average particle size is 10.1 ± 0.4 nm, which is even lower than that of PtPd catalyst. These results highlight an efficient deposition of both metallic phase combinations within the micropores of the ACP support despite the different loading of each one. Hence, well-dispersed nanoparticles with small sizes are obtained in both cases by simultaneous incipient wetting methodology.

Activated carbon shows poorer acidic properties than HZSM-5 zeolites (Table 1), displaying similar total acidity values to those of the less acidic Z140 zeolite. The zeolite with the lowest Si/Al ratio (Z15) exhibits the highest total acidity ($0.82 \text{ mmol}_{\text{tBA}} \text{ g}_{\text{cat}}^{-1}$), being at least two times higher than those of the other samples. Moreover, the Z140 and Z15 zeolites show average acidic strength values of 112 and 150 kJ mol_{tBA}⁻¹, respectively, whereas ACPs reach a maximum of 70 kJ mol_{tBA}⁻¹. This result points out that the acidic sites formed by the substitution of Si atoms for Al ones in the zeolite framework are stronger than the stable –C–O–P–OH acid structures of the ACP support [36].

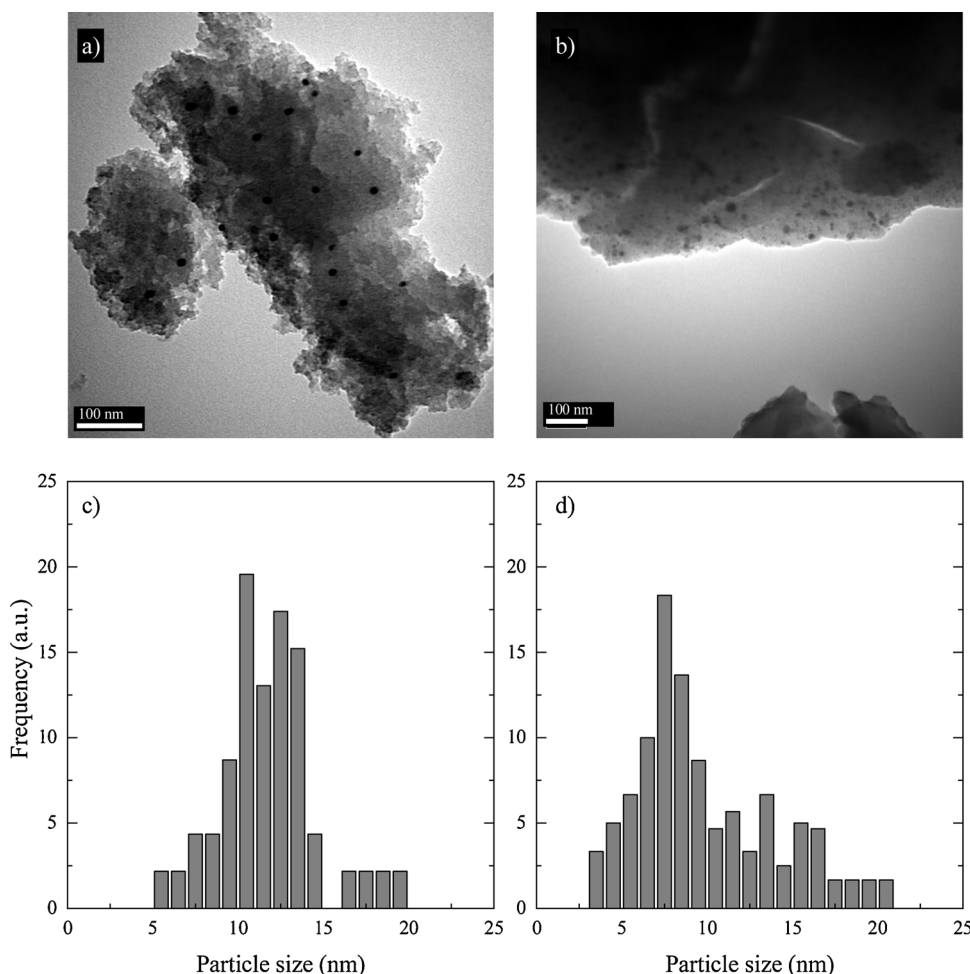


Fig. 1. TEM images and metal particle size distribution for the fresh a,c) PtPd and b,d) NiW catalysts.

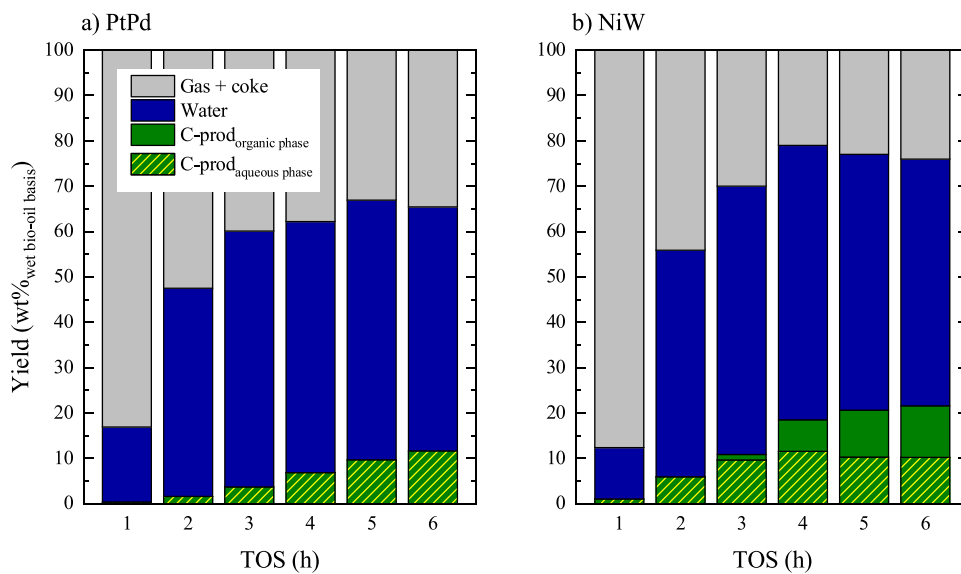


Fig. 2. Evolution with TOS of the main product yields (in a wet bio-oil basis) obtained using the a) PtPd and b) NiW catalysts.

3.2. Comparative of the performance of the PtPd and NiW catalysts with time on stream

The main product yields (carbon products, water, and gas + coke, calculated as stated in Eq. (1)) on a full bio-oil basis for the PtPd and NiW catalysts are displayed in Fig. 2 for a time on stream (TOS) of 0–6 h. For both catalysts, a predominant production of water was observed (46–59 wt%) at TOS > 2 h, together with a parallel decrease in the gas + coke yield and increasing carbon product formation. Interestingly, for a given time on stream, the amount of carbon products obtained with the PtPd catalyst (Fig. 2a) were approximately half the amount than those obtained with the NiW catalyst (Fig. 2b), with yields of 0.0–11.6 wt% and 1.1–21.6 wt%, respectively. Gas and coke formation occurred in a lesser extent using the NiW catalyst, due to its lower cracking activity. The lower acidity of this catalyst (0.28 mmol_{cat}⁻¹, see Table 1) plays an important role in this regard, limiting cracking reactions that lead to gas products as previously observed by Ibáñez et al. [42] in the cracking/deoxygenation of bio-oil into hydrocarbons. Regarding carbon product yields, it was also observed that using the PtPd catalyst all carbon products were originated from an aqueous liquid product phase, as a consequence of the high HDO activity of this catalyst [43], while an organic product fraction was also detected in the liquid products at TOS > 2 h using the NiW catalyst, providing with about 50% of the total carbon products. In addition, Pd is known to act as a promoter for hydrogenation reactions in Pt-based catalysts [44], hence leading to lighter products more likely to be gaseified.

Interestingly, the most favorable operating conditions (higher liquid carbon product yields) were attained at TOS = 6 h in deactivated catalyst conditions, and once a pseudosteady state of the catalyst was reached. This result evidences that in the catalyst deactivation period, the reactions which favor the formation of subproducts are selectively affected. Comparing the results for both catalysts and aiming for higher yields of carbon products, the use of the NiW catalyst is the most adequate, with a low acidity and a moderately active metallic phase. In addition, the results corroborate the hydrothermal stability of the ACP support in a reaction medium with a high steam content, as previously demonstrated by Bedia et al. on dehydration reactions for alcohols [37,45].

Focusing on the carbon liquid products, Fig. 3 shows the evolution with time on stream of the main lumps on a dry bio-oil basis (as defined in Eq. (2)) for the two ACP-based catalysts, until both reach a constant activity. A clear predominance of the lump of oxygenates (comprising

methanol, acetone and acetic acid) was observed in both cases, increasing with time on stream up to 6.2 wt% and 16.0 wt% in the case of the PtPd (Fig. 3a) and NiW catalysts (Fig. 3b), respectively. While using the PtPd catalyst, phenol and alkylphenolic component yields remain very low (< 1 wt%) with negligible amounts of the rest of the products. This is a consequence of a significant formation of water, which accounted for 93.2–98.0 wt% of the total aqueous phase (Fig. S2), providing low amounts of desired chemicals. On the other hand, for the NiW catalyst yields up to 3.8 wt% phenol, 10.5 wt% total aromatics (3.6 wt% A₁ and 6.9 wt% A₂), 5.3 wt% ketones and lesser amount of alkanes (1.2 wt%) were obtained at TOS = 6 h. These significantly higher yields are primarily a consequence of the aforementioned lower dehydration and cracking activity of the NiW catalyst (eventually leading to less water being formed, 84.2–91.7 wt%, see Fig. S2) causing the formation of an organic liquid product fraction, as discussed for Fig. 2b. It was observed that for this catalyst both the aqueous and organic liquid phases are a rich source for components of interest. This way, phenol yields increase steadily during the whole reaction, whereas the yields of aromatics, ketones and alkanes increase mainly at TOS > 3 h once the organic liquid product phase begins to form. The steady increase of the phenol and phenolic compound yields over time reflects a loss of the dehydration and cracking activity of the catalysts, which are also in line with the lower gas product formation at higher TOS values (see Fig. 2) and the steady drop in the water content in the aqueous phase (Fig. S2). However, despite its overall lower HDO activity, the NiW catalyst still displays a certain dehydroxylation capacity over time on stream, capable of removing the –OH functionalities from phenolic compounds, leading to significant amounts of aromatic compounds. It should also be mentioned that, when the production of phenolic and aromatic monomers (A₁) is targeted, there is an interest for operating at high temperatures, hence producing a favorable synergistic effect for displacing the hydrogenation equilibrium [9]. Dehydrogenation and condensation of aromatics also gives way to the formation of higher aromatics (A₂), known to be important precursors in the formation of coke [46]. The higher microporosity of the PtPd catalyst (Table 1) is also likely playing an enhancing role with regard to the formation of bulkier products prone to being trapped within narrow pores and further evolving into less hydrogenated structures, ultimately causing micropore blockage [23,47].

Fig. S3 shows the relative composition of the three components grouped in Fig. 3 in the oxygenates product lump: methanol, acetone and acetic acid. Using the PtPd catalyst (Fig. S3a) the oxygenates fraction mainly consisted of methanol (76–89 wt%) with lower amounts

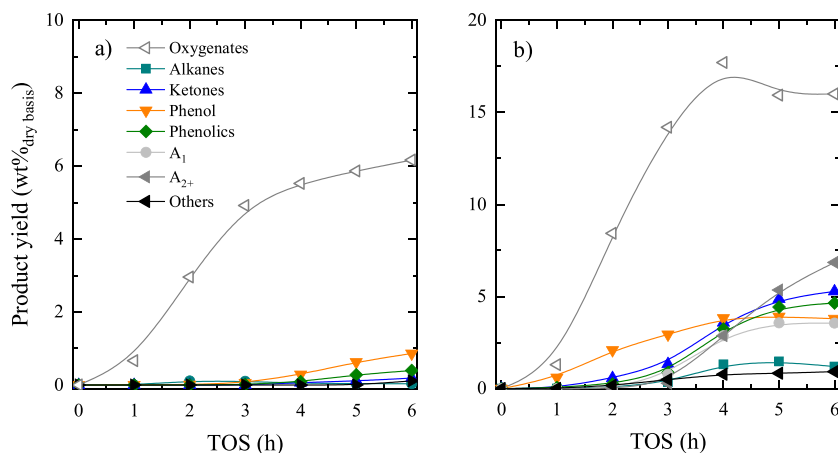


Fig. 3. Evolution with TOS of the main liquid carbon lump yields using the a) PtPd and b) NiW catalysts.

of acetone (7–11 wt%) and minor amounts of acetic acid (1–5 wt%), increasing up to 12 wt% at TOS = 6 h). This great formation of methanol on the aqueous phase was previously observed [9], highlighting the potential interest of this aqueous phase for being co-fed in the methanol-to-olefins (MTO) process. On the other hand, a predominance of acetic acid (56–72 wt%) in the oxygenates product lump was observed with the NiW catalyst (Fig. S3b) at TOS > 1 h, with a concentration of 10–13 wt% of acetone and 19–29 wt% methanol, with the exception of TOS = 1 h, where methanol was the main component (67 wt%). These different compositions of the oxygenates product lump are indicative of the distinct activity of the two ACP-based catalysts, again evidencing a higher HDO capacity for the PtPd catalyst, which is also in agreement with the higher phenol amounts formed using the NiW catalyst (Fig. 3b). This significant formation of methanol originates mainly from the C–O bond cleavage of ester compounds [9] and demethoxylation reactions of alkylmethoxy phenols, which are known to be heavily present in biomass-derived pyrolysis oils [48].

In concordance with the composition of the oxygenates lump, the analysis of the gas products (Fig. S4) evidenced a significantly higher concentration of CO and CH₄ (35.8 vol% and 15.3 vol%, respectively) when using the PtPd catalyst, originating from the cracking of oxygenates. CO₂ was the main compound in the gas products formed using the NiW catalyst (31.4 vol%), forming mainly from the decarboxylation of acetic acid, which decomposes catalytically through a competitive decarboxylation–dehydration mechanism, releasing CO₂ and CH₄ [49].

3.3. Effect of the addition of a physically mixed zeolite with the ACP-based catalysts

As discussed earlier, when dealing with biomass-derived feedstock, there is a known capacity of the HZM-5 zeolite towards forming aromatic components from other hydrocarbon and oxygenates [29,50]. The shape selectivity of this zeolite presents little diffusion restrictions for the oxygenates in bio-oil. In this section, the performance of the ACP-based catalysts alone was compared with that of physical mixtures of these catalysts (80 wt%) with HZSM-5 zeolites (20 wt%) of different Si/Al ratio (Si/Al = 15 and 140, denoted as Z15 and Z140, respectively).

The product distribution (on a wet bio-oil basis) obtained with the different physical mixtures of the catalysts are displayed in Fig. 4. As observed for the ACP-based catalysts alone (see Fig. 2), water was also the main product, attaining slightly higher yields when the Z15 zeolite was used in the mixture: 61.7 wt% and 62.2 wt% with the PtPd and NiW catalyst, respectively, in contrast to 53.0 wt% and 56.0 wt% obtained with the Z140 zeolite in the mixture. This greater water formation is explained by a higher hydrodeoxygenation and cracking capacity provided by the higher acidity and acidic strength of the Z15

zeolite, which doubles that of the Z140 zeolite (see Table 1). The synergistic effect of the zeolite in the mixture promotes cracking reactions, tending to form lighter components that will likely hydrogenate fast. Hence, a higher oxygen removal is attained, ultimately leading to a greater water formation.

Interestingly, when physically mixing zeolites with the PtPd catalyst, an organic product phase was detected, opposite to what occurred when operating with the PtPd catalyst alone (Fig. 2a), evidencing an acid-catalyzed enhancement of deoxygenation and aromatization-condensation reaction pathways. Organic products were formed at TOS > 3 h using all catalyst combinations with the exception of the PtPd + Z15 mixture (Fig. 4b), where organic product appear at TOS > 5 h. These results corroborate the higher cracking activity of the most acidic zeolite. This different acidity of the zeolites also explains the much greater content of organic products obtained with the NiW + Z140 mixture (accounting for 62.2% of the total carbon products) in comparison with the NiW + Z15 combination (36.2 wt% of total carbon products).

From all these results, the preference of using a less acidic zeolite (of a higher Si/Al ratio) in combination with a mildly active metallic phase (Ni–W) in this hydroprocessing approach is evidenced, directing the process towards enhanced yields of carbon products.

A detailed comparative of the evolution with time on stream (TOS) of the carbon product yields (on a dry basis) for all the catalyst combinations (ACP-based alone and the ACP + zeolite mixtures) is provided in Fig. 5. In this case, the physical mixtures with the Z140 zeolite provided carbon-product yields about 2–5 wt% higher than the ACP-based catalysts alone while, on the contrary, the mixtures with the Z15 zeolite led to overall lower carbon product yields than their ACP-based counterparts alone. Specifically, at TOS = 5 h, when the organic phase began to form using the PtPd + Z15 mixture, a pronounced increase in the carbon product yield was observed, eventually leading to slightly higher yields in comparison with the PtPd catalyst at TOS = 6 h. This indicates that despite the higher initial activity of the PtPd + Z15 combination there is an increased effect of the catalyst deactivation, ultimately causing a greater activity loss than for the rest of the catalysts.

The evolution of the turnover number (TON) over time on stream, depicted in Fig. S5 (as defined per mg of metal in the catalyst and mmol of acidic site), further demonstrates the increasing capacity of all their catalysts for yielding carbon products (specially the ACP-based mixtures with the Z140 zeolite) with analogue trends to those observed in Fig. 5.

The yields of the different carbon product lumps (on a dry basis) at TOS = 6 h for the ACP-based catalysts and mixtures with zeolites are displayed in Fig. 6. As previously depicted in Fig. 4a, the mixtures of the ACP-based catalyst and the zeolites (Fig. 6a) are selective catalysts for

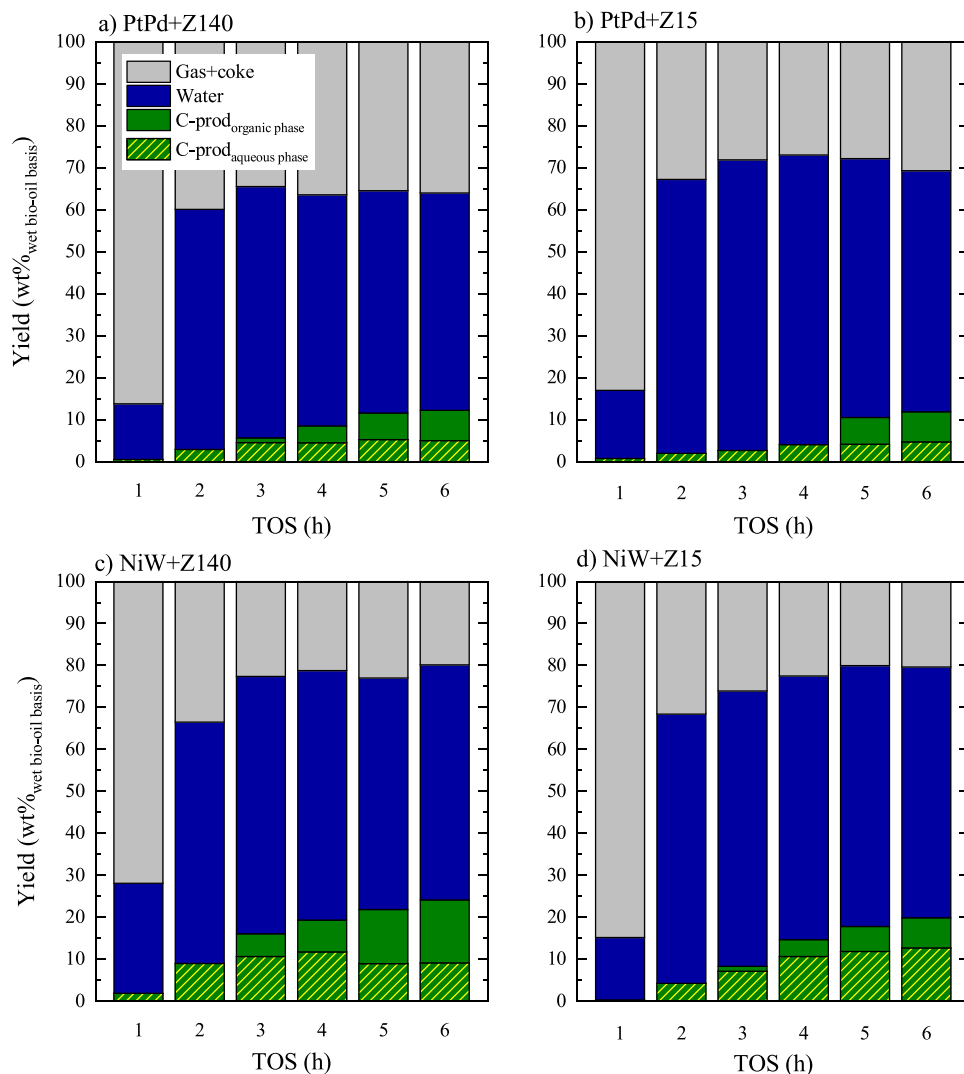


Fig. 4. Evolution with TOS of the main product yields (in a wet basis) obtained using the a,b) PtPd and c,d) NiW catalysts.

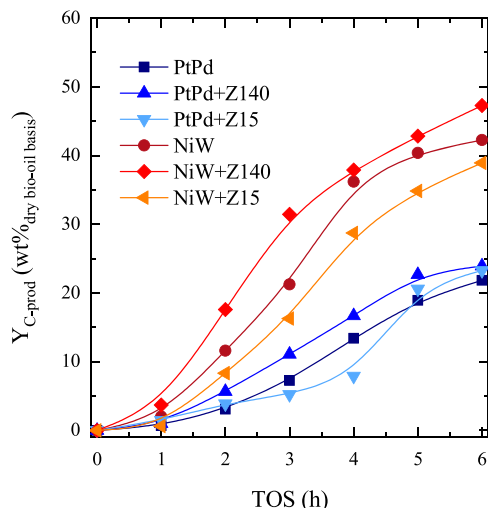


Fig. 5. Evolution with TOS of the total carbon product yield (on a dry basis) for the PtPd and NiW catalysts and their zeolite mixtures.

HDO reactions, which led to the formation of an organic phase, hence observing a pronounced increase in the yields of mostly aromatic components (8.3–8.7 wt% total aromatics) and alkanes (2.3–3.1 wt%),

compared with the performance of the PtPd catalyst alone (see Fig. 2a). In contrast, regarding the NiW catalyst (Fig. 6b), an improvement in the phenol and aromatic component yields was only observed when mixed with the Z140 zeolite, while mixtures with the Z15 zeolite resulted in comparatively lower yields of all the hydrocarbon lumps with exception of the oxygenates (which increased up to 19.4 wt%). The enhancing effect for the production of aromatics using HZSM-5 zeolites (Si/Al = 15 and Si/Al = 40, designated as Z15 and Z40, respectively) was previously reported by Valle et al. on the cracking/deoxygenation of bio-oil/methanol mixtures into hydrocarbons, were the most acidic Z15 zeolite proved to be more selective towards the production of aromatics, while the mildly acidic Z40 led primarily to olefins [51].

3.4. Catalyst deactivation

In order to explain catalyst deactivation and understand its effect on conversion and product distribution, used catalysts were characterized by means of different techniques. The obtained DTG-TPO profiles for the used PtPd and NiW catalysts and their physical mixtures with the Z140 and Z15 zeolites are depicted in Fig. 7a and b, respectively. These catalysts are the ones used in the previous section at TOS = 6 h. The DTG-TPO profiles corresponding to the fresh PtPd (Fig. 7a) and NiW (Fig. 7b) catalysts are also provided. A defined peak at ca. 515 °C is observed for the fresh catalysts, corresponding to the combustion of the ACP support. Even though higher combustion temperatures were

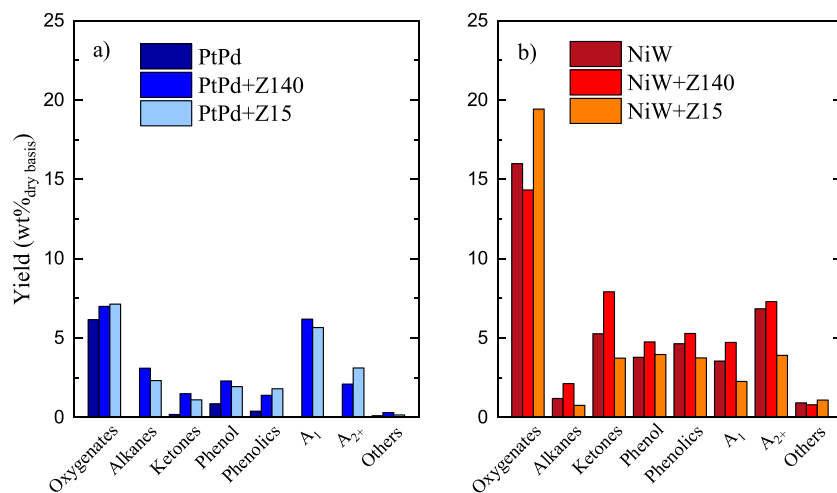


Fig. 6. Comparison of the main product yields at TOS = 6 h for the a) PtPd and b) NiW catalysts and their zeolite mixtures.

previously reported for these P-containing activated carbons [52], the presence of the metallic phase promotes the combustion of the ACP support at lower temperatures [47]. In the case of used catalyst, three peaks are registered, which are attributable to the combustion of different species (detailed deconvolution profiles are provided for two used catalyst samples in Fig. S6) [23]: (i) thermal lignin (TL, at ca. 385 °C), formed mainly from repolymerization of the phenolic components in bio-oil and which burns at low temperature due to its location on the outside of the catalyst particles; (ii) catalytic coke (CK, at ca. 445 °C), deposited over the metallic sites and whose formation is activated by these sites and the acidic ones and; (iii) the ACP support (ACP, at ca. 515 °C) [23]. The DTG-TPO profiles of all used catalysts were deconvoluted according to this classification and the obtained values of total amount of coke (TL + CK) and of each fraction (TL, CK and ACP) are listed in Table 2. The total coke content is higher in the PtPd catalyst and its mixtures (53.1–74.1 wt%) and reaches a maximum of 74.1 wt% with the used PtPd + Z15 combination. The NiW-containing catalysts present amounts of coke between 34.1 and 38.9 wt%. Interestingly, the minimum content of coke among all catalysts is registered for the NiW + Z15, with less than half amount than its PtPd counterpart (34.1 wt%).

Regarding the results of the used ACP-based catalysts alone, the species deposited on the surface of the PtPd catalyst present a more

heterogeneous composition and thus, its DTG-TPO profile does not show well-defined peaks (Fig. 7a). On the other hand, the NiW catalyst clearly shows a narrow peak associated with the combustion of TL, besides that corresponding to the combustion of the ACP support (Fig. 7b). This could be related to the higher abundance of phenols and (alkyl)phenolics in the reaction medium (see Fig. 3), which tend to thermally repolymerize. Hence, the higher activity of the PtPd catalyst promotes the development of CK structures by condensing the coke precursors [23]. Thereby, the CK/TL ratios are 1.2 and 0.8 for the PtPd and NiW catalysts, respectively (Table 2). All in all, it can be concluded that both the different reaction medium composition and HDO activity of the catalysts seems to play an important role in their contribution to each deactivation pathways. In addition, the more microporous structure of PtPd catalyst is also likely trapping aromatic coke structures within its narrower pores, leading to higher coke contents being deposited, as reported in Table 2.

The incorporation of HZSM-5 zeolites in the catalyst bed enhances the proportion of the CK fraction with respect to the deposited TL, highlighting the importance of the reaction medium composition and the activity of the catalysts in coke formation reactions. Overall, the PtPd-based catalytic systems exhibit higher amount of deposited coke than the NiW counterparts. A clear tendency is observed among the PtPd-based systems, with increasing amounts of CK (and higher CK/TL

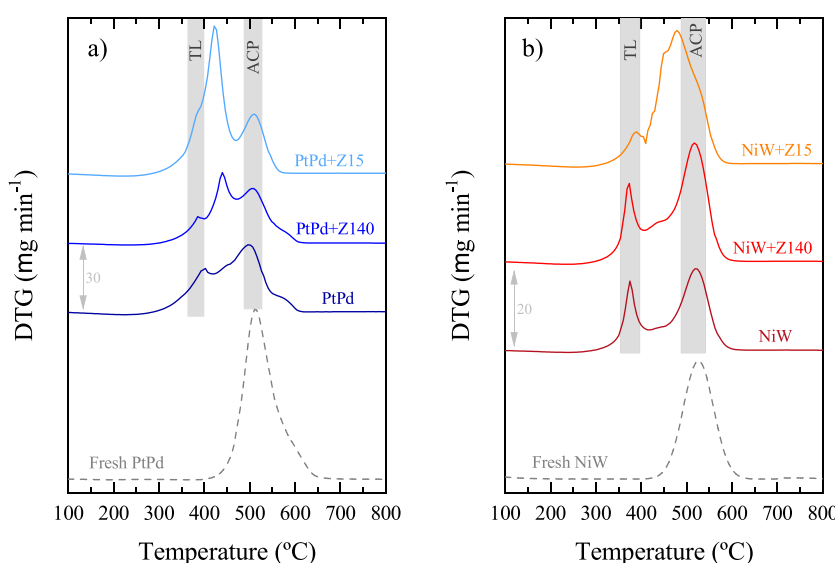


Fig. 7. DTG-TPO profiles for the combustion of the fresh and used a) PtPd and b) NiW catalysts and their zeolite mixtures.

Table 2

Total coke contents, relative contents of coke fractions (DTG-TPO profile deconvolution value) and C/O ratio (from XPS analysis) of the used catalysts.

	Coke (wt%)	TL (wt%) (385 ± 11) °C	CK (wt%) (445 ± 20) °C	ACP (wt%) (515 ± 9) °C	CK/TL	C/O
PtPd	60.7	27.0	33.7	39.3	1.2	6.6
PtPd + Z140	53.1	8.1	44.9	46.9	5.5	5.2
PtPd + Z15	74.1	11.5	62.6	25.9	5.5	9.8
NiW	38.9	21.2	17.7	61.2	0.8	6.8
NiW + Z140	35.0	18.7	16.3	65.0	0.9	5.9
NiW + Z15	34.1	4.5	29.6	65.9	6.6	12.9

ratio) upon addition of the zeolites (of higher acidity), as a consequence of the enhancement of condensation and dehydration reactions, which lead to the formation of bulky aromatic coke precursors. On the other hand, the NiW-based systems formed similar amounts of coke, and from the values reported in Table 2, we observed that the addition of the Z140 zeolite to the NiW catalyst does not present a clear influence nor on the total content neither on the composition of coke. On the contrary, coke composition is clearly modified by the Z15 zeolite although the total amount of deposits remains similar. In this regard, the significantly higher acidity of the Z15 zeolite (see Table 1) compared to the acidity of Z140 (similar to that of the ACP supports) does not seem to affect the side reactions that lead to the formation of CK to a great extent.

Comparing the behavior of the Z140-containing systems, the aforementioned poorer HDO performance of NiW metallic phase, with lower capacity for the production deoxygenated hydrocarbons, does not favor the condensation due to its low acidity. Otherwise, when mixing the ACP-based catalysts with the more acidic Z15 zeolite (higher activity towards dehydration), condensation reactions of the CK precursors are also favored over the strong acidic sites of this zeolite (Table 1), which raises the values of CK/TL ratio up to 5.5 and 6.6 for the used PtPd + Z15 and NiW + Z15 catalyst mixtures, respectively (Table 2).

The two carbonaceous species identified in the combustion of the used catalysts (see Fig. 7), namely TL and CK, also present compositional differences and, while CK is mainly formed by polycyclic aromatic structures of carbon atoms, TL presents O-containing functionalities and polyphenolic chains [32,53]. In order to corroborate the discussed composition of these species based on TG-TPO results, XPS analyses of the used catalysts were carried out, and Table 2 shows the estimated C/O ratio of each one. Comparing these ratios with those of the fresh PtPd and NiW catalysts of 10.5 and 6.5, respectively (calculated from the data in Table 1), in most cases, a decrease in this ratio is observed for used catalyst as a consequence of a significant presence of O-containing TL. Comparing the values of the used ACP-based catalysts alone and those of the physical mixtures with Z140 zeolite, a slight drop of the oxygen content is observed. However, the addition of Z15 zeolite boosts the carbon content, obtaining C/O ratio values of 9.8 and 12.9 for the used PtPd + Z15 and NiW + Z15 catalyst mixtures. This result is consistent with the high proportion of CK deposited in these cases, determined by TG-TPO experiments.

The physico-chemical properties of used catalysts are listed in Table 3. Two clearly differentiated results can be observed regarding the effect of coke deposition on the textural parameters of catalysts. The used PtPd catalyst, its combination with Z140 zeolite and the NiW + Z15 combination show little remaining porous structure with very low values of V_{micr} and V_{mes} (0.02 and $0.07 \text{ cm}^3 \text{ g}^{-1}$, respectively, for the used PtPd catalyst). It should be mentioned that these mixtures present a marked contribution of CK ($\text{CK/TL} > 1$ in Table 2), which is presumably formed within the micropores. On the contrary, the used catalysts that exhibit values of $\text{CK/TL} < 1$ (namely NiW and NiW + Z140) present completely blocked pores and negligible values of S_{BET} , mainly attributable to the external surface area (S_{ext} of 32 and $51 \text{ m}^2 \text{ g}^{-1}$, respectively). Interestingly, they exhibit measurable narrow

micropore areas (S_{DR}) which was elsewhere ascribed to the TL porosity [23]. This total blockage, alongside the low combustion temperature of TL (Fig. 7), corroborates the deposition of TL on the external surface of the catalyst, clogging pore entrances. Finally, the elevated content of deposits in the used PtPd + Z15 combination (74.1 wt%) also leads to a total pore blockage, which is barely measurable by means of N_2 adsorption-desorption. This significantly high coke content of the PtPd + Z15 combination is in agreement with the high acidity and acidic strength of the Z15 zeolite and the greater activity loss previously discussed in Fig. 5, which was accentuated at $TOS > 4 \text{ h}$.

Furthermore, the deposition of carbon structures on the catalyst provokes a pronounced decrease in the surface concentration of metals, as observed from the XPS data also provided in Table 3. A significant decrease in the Pt-Pd and Ni-W apparent surface concentrations is registered in all cases, with values between 0.1 and 0.3 wt% of Pt, Pd or W and a maximum of 1.0 wt% of Ni in the NiW + Z15 combination. This can be explained from the deposition of coke over the metallic sites of the catalyst, which hinders the identification of metals through XPS. A significant decrease in the P apparent surface concentration from values of 2.4 and 1.9 wt% for the fresh catalysts (see Table 1) is also noteworthy. Since surface P groups were previously associated with the acidity of the ACP support [9], the decrease of accessible P on the carbon surface can be related with the activity loss of the ACP support acidic sites.

The C1s, O1s, P2p, Pt4f, Pd3d, Ni2p and W4f XPS spectra of fresh and used catalysts are provided in Fig. S7 of Supporting material. The C1s peak (Fig. S7a,b) has been established at 284.5 eV and used as reference for locating all the peaks. As expected, an almost unimodal distribution is observed with the peak centered at this binding energy (attributed to the graphitized structures of both the support and the deposited species). A small hump at ca. 290 eV, attributable to carboxyl or carbonate functional groups [54], is also observed for the fresh catalysts, but non-detectable in the used catalysts. On the other hand, interesting shifts are observed in the O1s spectrum with both catalysts after the reaction (Fig. S7c and d). On the one hand, fresh catalysts exhibit a significant contribution of the functional groups located at 532–531 eV associated with C=O and P=O support functionalities and with Metal-O bonds [54]. On the other hand, the increase in the total amount of O1s is directly related to species in the binding energy range of 533–534 eV, corresponding to phenolic (C-OH) and C-O-C bonds [53]. These functionalities have been associated with the structure of TL, suggesting that the increase in O1s is due to the deposition of this type of deactivating species. Indeed, the addition of the Z140 catalyst, which leads to the formation of a coke with the lowest C/O ratio in the case of both catalysts (Table 2), also leads to the sharpest and most pronounced shifts of the spectrum towards higher binding energies. Similarly, the remaining P functionalities of the support also show more oxidized states (Figs. S7e and f), confirming the great affinity of this groups for oxygen in an oxygen-rich medium. Nevertheless, the signal of P is negligible in most cases due to the high amount of deposited carbonaceous species during the reaction. This effect is accentuated in the case of the active metals, being the signal of Pt4f, Pd3d, Ni2p and W4f too weak for a rigorous discussion of the results (Fig. S7g–j).

It should be noted that the severe deterioration of the catalyst

Table 3

Physico-chemical properties of the used catalysts.

	PtPd	PtPd + Z140	PtPd + Z15	NiW	NiW + Z140	NiW + Z15
Textural parameters						
$S_{\text{BET}} (\text{m}^2 \text{g}^{-1})$	72	93	1	2	3	10
$V_{\text{micr}} (\text{cm}^3 \text{g}^{-1})$	0.02	0.03	–	–	–	–
$V_{\text{mes}} (\text{cm}^3 \text{g}^{-1})$	0.07	0.07	0.01	0.01	0.01	0.02
$S_{\text{ext}} (\text{m}^2 \text{g}^{-1})$	36	34	1	2	4	9
$S_{\text{DR}} (\text{m}^2 \text{g}^{-1})$	46	52	40	32	51	61
XPS surface concentration						
P (wt%)	0.3	1.6	0.1	0.4	0.2	0.9
Pt (wt%)	0.2	0.3	0.1	–	–	–
Pd (wt%)	0.2	0.2	0.2	–	–	–
Ni (wt%)	–	–	–	0.4	0.1	1.0
W (wt%)	–	–	–	0.1	0.1	0.2

porous structure, as a consequence of a significant coke deposition, is not in agreement with the fact that at TOS = 6 h the catalysts maintain a notable HDO activity. This apparent contradiction can be explained by the different state of the coke in reaction conditions and the conditions at which the N₂ adsorption-desorption analysis is carried out. The remaining catalyst activity (and the fact that it is kept constant) implies that the pore structure of the ACP support and the HZSM-5 zeolite are not completely blocked by coke under reaction conditions, at elevated temperature and under high flows of H₂ and steam.

4. Conclusions

The good performance of two different PtPd and NiW bifunctional catalysts supported on a phosphorus-containing activated carbon (ACP) on the hydrodeoxygenation (HDO) of a raw black poplar bio-oil was demonstrated. The stability of these catalysts after an initial deactivation period due to coke deposition outstands after 6 h of time on stream. In this pseudosteady state conditions, and with moderate dehydration and cracking activity, the NiW catalyst shows a good behavior in the reactions involved in HDO, with a 42.3 wt% carbon product yield (in a dry bio-oil basis), containing 5.3 wt% phenolic and 12.3 wt% aromatic components.

The addition of physically mixed HZSM-5 zeolites into the catalytic bed (20 wt%) also enhances the yield of the organic liquid product fraction. Nevertheless, the acidity of the zeolite has a strong influence on the results. A maximum carbon product yield (25 wt% on a dry basis) rich in phenolic and aromatic components (8 and 15 wt% in dry basis, respectively) is achieved using a less acidic zeolite with a higher Si/Al ratio (Si/Al = 140) together with the NiW catalyst, whereas an increase in the zeolite acidity (Si/Al = 15) has a negative impact by boosting the production of water, gas products and coke. This is a consequence of the promotion of acid-catalyzed dehydration and cracking reactions.

Two different species of coke are identified as responsible for catalyst deactivation, one of them arising from thermal mechanisms (thermal lignin, TL) and another one with a catalytic origin (catalytic coke, CK). TL is mainly evolving from repolymerization of unstable (alkyl)phenolic compounds in bio-oil, and therefore is predominant on the external surface of catalyst. The higher conversion of these bio-oil oxygenates with the PtPd catalyst presents the secondary effect of favoring the development of CK within the porous structure of the ACP through a mechanism of acid-catalyzed condensation reactions. The presence of a HZSM-5 zeolite with a high acidity (Z15) promotes these condensation reactions of coke formation, significantly increasing the CK/TL ratio (up to 6.6). This internal coke (CK) deposition phenomenon is attenuated by using a combination of the NiW catalyst and Z140 zeolite, due to their moderate acidity. This stable combination provides encouraging results in the production of added-value chemicals.

Declaration of Competing Interest

The authors declare that they have no known competing financial interests or personal relationships that could have appeared to influence the work reported in this paper.

Acknowledgements

This work was carried out with the support of the Ministry of Economy and Competitiveness of the Spanish Government, some co-founded with ERDF funds (CTQ2015-67425-R and CTQ2015-68654-R), the Basque Government(IT1218-19) and the European Commission (Horizon H2020-MSCA RISE-2018, Contract No. 823745). Dr. Idoia Hita is grateful for her postdoctoral grant awarded by the Department of Education, University and Research of the Basque Government (POS_2015_1_0035).

Appendix A. Supplementary data

Supplementary material related to this article can be found, in the online version, at doi:<https://doi.org/10.1016/j.apcatb.2019.118112>.

References

- [1] M. Patel, X. Zhang, A. Kumar, Techno-economic and life cycle assessment on lignocellulosic biomass thermochemical conversion technologies: a review, Renew. Sustain. Energy Rev. 53 (2016) 1486–1499.
- [2] G.W. Huber, S. Iborra, A. Corma, Synthesis of transportation fuels from biomass: chemistry, catalysts, and engineering, Chem. Rev. 106 (2006) 4044–4098.
- [3] A. Oasmaa, S. Czernik, Fuel oil quality of biomass pyrolysis oils—state of the art for the end users, Energy Fuels 13 (1999) 914–921.
- [4] E. Lazzari, T. Schema, M.C.A. Marcelo, C.T. Primaz, A.N. Silva, M.F. Ferrão, T. Bjerk, E.B. Caramão, Classification of biomass through their pyrolytic bio-oil composition using FTIR and PCA analysis, Ind. Crops Prod. 111 (2018) 856–864.
- [5] A. Remiro, A. Arandia, L. Oar-Arreta, J. Bilbao, A.G. Gayubo, Regeneration of NiAl₂O₄ spinel type catalysts used in the reforming of raw bio-oil, Appl. Catal. B Environ. 237 (2018) 353–365.
- [6] L. Santamaría, G. López, A. Arregi, M. Amutio, M. Artetxe, J. Bilbao, M. Olazar, Stability of different Ni supported catalysts in the in-line steam reforming of biomass fast pyrolysis volatiles, Appl. Catal. B Environ. 242 (2019) 109–120.
- [7] B. Valle, A. Remiro, N. García-Gómez, A.G. Gayubo, J. Bilbao, Recent research progress on bio-oil conversion into bio-fuels and raw chemicals: a review, J. Chem. Technol. Biotechnol. 94 (2018) 670–689.
- [8] W. Yin, R.H. Venderbosch, H.J. Heeres, 8—Recent developments in the catalytic hydrotreating of pyrolysis liquids, in Direct Thermochem., Liq. Energy Appl. (2018) 249–292.
- [9] T. Cordero-Lanzac, R. Palos, J.M. Arandes, P. Castaño, J. Rodríguez-Mirasol, T. Cordero, J. Bilbao, Stability of an acid activated carbon based bifunctional catalyst for the raw bio-oil hydrodeoxygenation, Appl. Catal. B Environ. 203 (2017) 389–399.
- [10] K.A. Resende, C.A. Teles, G. Jacobs, B.H. Davis, D.C. Cronauer, A.J. Kropf, C.L. Marshall, C.E. Hori, F.B. Noronha, Hydrodeoxygenation of phenol over zirconia supported Pd bimetallic catalysts. The effect of second metal on catalyst performance, Appl. Catal. B Environ. 232 (2018) 213–231.
- [11] A. Gutiérrez, J.M. Arandes, P. Castaño, M. Olazar, J. Bilbao, Effect of pressure on the hydrocracking of light cycle oil with a Pt-Pd/HY catalyst, Energy Fuels 26 (2012) 5897–5904.
- [12] K.A. Resende, A.H. Braga, F.B. Noronha, C.E. Hori, Hydrodeoxygenation of phenol

- over Ni/Ce_{1-x}Nb_xO₂ catalysts, *Appl. Catal. B Environ.* 245 (2019) 100–113.
- [13] C.A. Teles, P.M. de Souza, A.H. Braga, R.C. Rabelo-Neto, A. Teran, G. Jacobs, D.E. Resasco, F.B. Noronha, The role of defect sites and oxophilicity of the support on the phenol hydrodeoxygenation reaction, *Appl. Catal. B Environ.* 249 (2019) 292–305.
- [14] M. Auersvald, B. Shumeiko, M. Staš, D. Kubička, J. Chudoba, P. Šimáček, Quantitative study of straw bio-oil hydrodeoxygenation over a sulfided NiMo catalyst, *ACS Sustain. Chem. Eng.* 7 (2019) 7080–7093.
- [15] X. Xtrine, M.H. Dabrosd, X. Xnagnus, Z. Stummamnd, X. Hejd, X. Xpeter, A. Jensem, X.-D. Grunwaldtd, X. Xjosten Gabrelsend, M. Mortensend, X. Xanker, D. Jensem, Transportation fuels from biomass fast pyrolysis, catalytic hydrodeoxygenation, and catalytic fast hydropyrolysis, *Prog. Energy Combust. Sci.* 68 (2018) 268–309.
- [16] P.J. de Wild, W.J.J. Huijgen, A. Kloekhorst, R.K. Chowdari, H.J. Heeres, Biobased alkylphenols from lignins via a two-step pyrolysis—hydrodeoxygenation approach, *Bioresour. Technol.* 229 (2017) 160–168.
- [17] D. Ballesteros-Plata, A. Infantes-Molina, M. Rodríguez-Cuadrado, E. Rodríguez-Aguado, P. Braos-García, E. Rodríguez-Castellón, Incorporation of molybdenum into Pt and Pt catalysts supported on commercial silica for hydrodeoxygenation reaction of dibenzofuran, *Appl. Catal. A Gen.* 547 (2017) 86–95.
- [18] W. Yin, R.H. Venderbosch, S. He, M.V. Bykova, S.A. Khromova, V.A. Yakovlev, H.J. Heeres, Mono-, bi-, and tri-metallic Ni-based catalysts for the catalytic hydrotreatment of pyrolysis liquids, *Biomass Convers. Biorefinery* 7 (2017) 361–376.
- [19] T.N. Phan, C.H. Ko, Synergistic effects of Ru and Fe on titania-supported catalyst for enhanced anisole hydrodeoxygenation selectivity, *Catal. Today* 303 (2018) 219–226.
- [20] I. Hita, T. Cordero-Lanzac, G. Bonura, C. Cannilla, J.M. Arandes, F. Frusteri, J. Bilbao, Hydrodeoxygenation of raw bio-oil towards platform chemicals over FeMoP/zeolite catalysts, *J. Ind. Eng. Chem.* (2019), <https://doi.org/10.1016/j.jiec.2019.08.019> In press.
- [21] A.A. Dwiamoko, L. Zhou, I. Kim, J.-W. Choi, D.J. Suh, J.-M. Ha, Hydrodeoxygenation of lignin-derived monomers and lignocellulose pyrolysis oil on the carbon-supported Ru catalysts, *Catal. Today* 265 (2016) 192–198.
- [22] S. Oh, H.S. Choi, I.-G. Choi, J.W. Choi, Evaluation of hydrodeoxygenation reactivity of pyrolysis bio-oil with various Ni-based catalysts for improvement of fuel properties, *RSC Adv.* 7 (2017) 15116–15126.
- [23] T. Cordero-Lanzac, R. Palos, I. Hita, J.M. Arandes, J. Rodríguez-Mirasol, T. Cordero, J. Bilbao, P. Castaño, Revealing the pathways of catalyst deactivation by coke during the hydrodeoxygenation of raw bio-oil, *Appl. Catal. B Environ.* 239 (2018) 513–524.
- [24] A. Sanna, T.P. Vispute, G.W. Huber, Hydrodeoxygenation of the aqueous fraction of bio-oil with Ru/C and Pt/C catalysts, *Appl. Catal. B Environ.* 165 (2015) 446–456.
- [25] C. Guo, K.T.V. Rao, Z. Yuan, S. (Quan) He, S. Rohani, C. (Charles) Xu, Hydrodeoxygenation of fast pyrolysis oil with novel activated carbon-supported NiP and CoP catalysts, *Chem. Eng. Sci.* 178 (2018) 248–259.
- [26] E. Santillan-Jimenez, M. Perdu, R. Pace, T. Morgan, M. Crocker, Activated carbon, carbon nanofiber and carbon nanotube supported molybdenum carbide catalysts for the hydrodeoxygenation of guaiacol, *Catalysts* 5 (2015) 424–441.
- [27] D.P. Serrano, J.A. Melero, G. Morales, J. Iglesias, P. Pizarro, Progress in the design of zeolite catalysts for biomass conversion into biofuels and bio-based chemicals, *Catal. Rev.* 60 (2018) 1–70.
- [28] M.M. Rahman, R. Liu, J. Cai, Catalytic fast pyrolysis of biomass over zeolites for high quality bio-oil—a review, *Fuel Process. Technol.* 180 (2018) 32–46.
- [29] B. Valle, A.G. Gayubo, A.T. Aguayo, M. Olazar, J. Bilbao, Selective production of aromatics by crude bio-oil valorization with a nickel-modified HZSM-5 zeolite catalyst, *Energy Fuels* 24 (2010) 2060–2070.
- [30] R. Shakya, S. Adhikari, R. Mahadevan, E.B. Hassan, T.A. Dempster, Catalytic upgrading of bio-oil produced from hydrothermal liquefaction of *Nannochloropsis* sp, *Bioresour. Technol.* 252 (2018) 28–36.
- [31] P.A. Lazaridis, A.P. Fotopoulos, S.A. Karakoulia, K.S. Triantafyllidis, Catalytic fast pyrolysis of kraft lignin with conventional, mesoporous and nanosized ZSM-5 zeolite for the production of alkyl-phenols and aromatics, *Front. Chem.* 6 (2018) 295.
- [32] B. Valle, P. Castaño, M. Olazar, J. Bilbao, A.G. Gayubo, Deactivating species in the transformation of crude bio-oil with methanol into hydrocarbons on a HZSM-5 catalyst, *J. Catal.* 285 (2012) 304–314.
- [33] F.H. Isikgor, C.R. Becer, Lignocellulosic biomass: a sustainable platform for the production of bio-based chemicals and polymers, *Polym. Chem.* 6 (2015) 4497–4559.
- [34] H. Zhang, Y. Wang, P. Zhang, X. Lin, Y. Zhu, Preparation of NiW catalysts with alumina and zeolite Y for hydroprocessing of coal tar, *J. Fuel Chem. Technol.* 41 (2013) 1085–1091.
- [35] R. Tong, Y. Wang, X. Zhang, H. Zhang, J. Dai, X. Lin, D. Xu, Effect of phosphorus modification on the catalytic properties of NiW/γ-Al₂O₃ in the hydrogenation of aromatics from coal tar, *J. Fuel Chem. Technol.* 43 (2015) 1461–1469.
- [36] M.J. Valero-Romero, F.J. García-Mateos, J. Rodríguez-Mirasol, T. Cordero, Role of surface phosphorus complexes on the oxidation of porous carbons, *Fuel Process. Technol.* 157 (2017) 116–126.
- [37] J. Bedia, R. Ruiz-Rosas, J. Rodríguez-Mirasol, T. Cordero, A kinetic study of 2-propanol dehydration on carbon acid catalysts, *J. Catal.* 271 (2010) 33–42.
- [38] A.R. Fernandez-Akarregi, J. Makibar, G. Lopez, M. Amutio, M. Olazar, Design and operation of a conical spouted bed reactor pilot plant (25 kg/h) for biomass fast pyrolysis, *Fuel Process. Technol.* 112 (2013) 48–56.
- [39] I. Hita, A. Gutiérrez, M. Olazar, J. Bilbao, J.M. Arandes, P. Castaño, Upgrading model compounds and scrap tires pyrolysis oil (STPO) on hydrotreating NiMo catalysts with tailored supports, *Fuel* 145 (2015) 158–169.
- [40] D. van Herk, P. Castaño, M. Quaglia, M.T. Kreutzer, M. Makkee, J.A. Moulijn, Avoiding segregation during the loading of a catalyst–inert powder mixture in a packed micro-bed, *Appl. Catal. A Gen.* 365 (2009) 110–121.
- [41] I. Hita, T. Cordero-Lanzac, A. Gallardo, J.M. Arandes, J. Rodríguez-Mirasol, J. Bilbao, T. Cordero, P. Castaño, Phosphorus-containing activated carbon as acid support in a bifunctional Pt-Pd catalyst for tire oil hydrocracking, *Catal. Commun.* 219 (2016) 48–51.
- [42] M. Ibáñez, B. Valle, J. Bilbao, A.G. Gayubo, P. Castaño, Effect of operating conditions on the coke nature and HZSM-5 catalysts deactivation in the transformation of crude bio-oil into hydrocarbons, *Catal. Today* 195 (2012) 106–113.
- [43] J. Wildschut, F.H. Mahfud, R.H. Venderbosch, H.J. Heeres, Hydrotreatment of fast pyrolysis oil using heterogeneous noble-metal catalysts, *Ind. Eng. Chem. Res.* 48 (2009) 10324–10334.
- [44] A. Gutiérrez, J.M. Arandes, P. Castaño, M. Olazar, J. Bilbao, Enhancement of aromatic hydro-upgrading on a Pt catalyst by promotion with Pd and shape-selective supports, *Fuel Process. Technol.* 101 (2012) 64–72.
- [45] J. Bedia, J.M. Rosas, J. Márquez, J. Rodríguez-Mirasol, T. Cordero, Preparation and characterization of carbon based acid catalysts for the dehydration of 2-propanol, *Carbon* 47 (2009) 286–294.
- [46] I. Hita, P.J. Deuss, G. Bonura, F. Frusteri, H.J. Heeres, Biobased chemicals from the catalytic depolymerization of Kraft lignin using supported noble metal-based catalysts, *Fuel Process. Technol.* 179 (2018) 143–153.
- [47] T. Cordero-Lanzac, I. Hita, A. Veloso, J.M. Arandes, J. Rodríguez-Mirasol, J. Bilbao, T. Cordero, P. Castaño, Characterization and controlled combustion of carbonaceous deactivating species deposited on an activated carbon-based catalyst, *Chem. Eng. J.* 327 (2017) 454–464.
- [48] L. Negahdar, A. Gonzalez-Quiroga, D. Otyuskaya, H.E. Toraman, L. Liu, J.T.B.H. Jastrzebski, K.M. Van Geem, G.B. Marin, J.W. Thybaut, B.M. Weckhuysen, Characterization and comparison of fast pyrolysis bio-oils from pinewood, rapeseed cake, and wheat straw using ¹³C NMR and comprehensive GC × GC, *ACS Sustain. Chem. Eng.* 4 (2016) 4974–4985.
- [49] D.C. Perera, J.W. Hewage, N. De Silva, Theoretical study of catalytic decomposition of acetic acid on MgO nanosurface, *Comput. Theor. Chem.* 1064 (2015) 1–6.
- [50] E. Kantarelis, W. Yang, W. Blasiak, Effect of zeolite to binder ratio on product yields and composition during catalytic steam pyrolysis of biomass over transition metal modified HZSM5, *Fuel* 122 (2014) 119–125.
- [51] B. Valle, A.G. Gayubo, A. Alonso, A.T. Aguayo, J. Bilbao, Hydrothermally stable HZSM-5 zeolite catalysts for the transformation of crude bio-oil into hydrocarbons, *Appl. Catal. B Environ.* 100 (2010) 318–327.
- [52] J.M. Rosas, R. Ruiz-Rosas, J. Rodríguez-Mirasol, T. Cordero, Kinetic study of the oxidation resistance of phosphorus-containing activated carbons, *Carbon* 50 (2012) 1523–1537.
- [53] A. Ochoa, B. Aramburu, M. Ibáñez, B. Valle, J. Bilbao, A.G. Gayubo, P. Castaño, Compositional insights and valorization pathways for carbonaceous material deposited during bio-oil thermal treatment, *ChemSusChem* 7 (2014) 2597–2608.
- [54] J.F. Moulder, W.F. Stickle, P.E. Sobol, K.D. Bomben, Jill Chastain (Ed.), *Handbook of X-ray Photoelectron Spectroscopy*, Perkin-Elmer Corporation, Minnesota (United States), 1995.